





## Geometry-induced rectification for an active object

Jae Sung Lee <sup>1,\*</sup>, Jong-Min Park <sup>1</sup>, Jae Dong Noh <sup>2</sup>, and Hyunggyu Park <sup>1,†</sup>

<sup>1</sup>*School of Physics, Korea Institute for Advanced Study, Seoul 02455, Korea*

<sup>2</sup>*Department of Physics, University of Seoul, Seoul 02504, Korea*



(Received 12 April 2021; accepted 18 October 2021; published 29 October 2021)

Studies of the rectified current induced by active particles have received great attention due to its possible application to a microscopic motor in biological environments. Insertion of an *asymmetric* passive object amid many active particles has been regarded as an essential ingredient for generating such a rectified motion. Here, we report that the reverse situation is also possible, where the motion of an active object can be rectified by its geometric asymmetry amid many passive particles. This may describe a unidirectional motion of apolar biological agents with asymmetric shape. We also find a weak but less dispersive rectified motion in a *passive* mode without energy pump-in. This “moving by dissipation” mechanism could be used as a design principle for developing more reliable microscopic motors.

DOI: [10.1103/PhysRevResearch.3.L042011](https://doi.org/10.1103/PhysRevResearch.3.L042011)

**Introduction.** Most biological systems are *active* in that they are self-propelled, i.e., driven by mechanical forces generated via an internal mechanism consuming chemical fuels [1]. This is in marked contrast to *passive* systems such as a Brownian particle, whose stochastic motions are governed by external reservoirs. The activeness leads to various unique features clearly distinguished from those of passive systems. For example, active systems show time-scale-dependent diffusivity due to colored noise [2–6], aggregation due to repulsive force [7], efficiency enhancement [8–10], and unconventional entropy production [10–14].

In much of the literature, this self-propelled motion has been encoded into velocity-dependent driving forces  $\mathbf{F}_{\text{drv}} = -\nabla_v \Phi(\mathbf{v})$  at the phenomenological level, where  $\mathbf{v}$  is the velocity of an active particle and  $\Phi(\mathbf{v})$  is a symmetric velocity potential. Specific examples are the Rayleigh-Helmholtz (RH) [15–17], depot [18–21], and Schienbein-Gruler (SG) models [22,23] proposed to describe the driving forces of various active systems such as molecular motors, bacteria, and moving cells, respectively. For each case, the driving force  $\mathbf{F}_{\text{drv}}$  is given by

$$\mathbf{F}_{\text{drv}} = -\Gamma(\mathbf{v})\mathbf{v}, \quad \text{with } \Gamma(\mathbf{v}) = \begin{cases} \hat{\gamma} + \omega v^2 & \text{RH} \\ \frac{\hat{\gamma}}{1+\zeta v^2} & \text{depot} \\ \hat{\gamma} v_0/|\mathbf{v}| & \text{SG,} \end{cases} \quad (1)$$

where  $v_0$  is a velocity unit defined in Eq. (5) and  $\hat{\gamma}$ ,  $\omega$ , and  $\zeta$  are tunable parameters. Here, we take  $\omega, \zeta > 0$  for

the stability, while  $\hat{\gamma}$  can be any real number. When  $\mathbf{F}_{\text{drv}}$  is applied to a particle with mass  $M$ , immersed in a liquid with friction coefficient  $\gamma > 0$  and temperature  $T$ , the steady-state velocity distribution is given by the exponential form  $\sim \exp[-M\tilde{\Phi}(\mathbf{v})/(k_B T \gamma)]$  with the effective potential  $\tilde{\Phi}(\mathbf{v}) \equiv \Phi(\mathbf{v}) + \gamma v^2/2$ . The driving force is denoted to be in the active (passive) mode when  $\tilde{\Phi}(\mathbf{v})$  is minimum at  $\mathbf{v} \neq 0$  ( $\mathbf{v} = 0$ ) [1]. In one dimension, the velocity distribution has symmetric double peaks in the active mode as shown by the left red curve in Fig. 1(a). These two peaks represent a nonzero self-propelling velocity. This active mode appears for  $\hat{\gamma} < \gamma_c$ , where  $\gamma_c = -\gamma$  for the RH and the depot models and  $\gamma_c = 0$  for the SG model. For  $\hat{\gamma} > \gamma_c$ , the velocity distribution becomes unimodal with no finite self-propelling velocity [see Fig. 1(a)], which indicates the passive mode. Note that the system is still out of equilibrium even in the passive mode due to the driving force. Even in the active mode, a self-propelled particle does not prefer any particular direction like in a standard run-and-tumble motion [1]; thus there exists no rectified motion (no net particle current) in the long-time limit. The zero current is a natural consequence of the symmetry of the effective potential,  $\tilde{\Phi}(\mathbf{v}) = \tilde{\Phi}(-\mathbf{v})$ .

In the meantime, the rectification of thermal fluctuations in a Brownian motor has been reported [24,25]. The essential ingredient for the nonzero current of the examples is the interplay of a nonequilibrium condition (temperature gradient) and a geometric asymmetry of the motor. Another interesting example is a “passive” ratchet surrounded by many “active” bacteria, which was found to exhibit a persistent rotational motion (rectified current) in recent experiments [26,27] and numerical simulations [28]. This triggered a flurry of subsequent research [29–35], due to a realistic applicability for designing a microscopic motor in biological environments. Note that this situation also combines nonequilibriumness (activity) and spatial asymmetry of the ratchet.

In this Research Letter, we introduce the reverse situation, where an asymmetric active particle is immersed in a

\*jslee@kias.re.kr

†hgpark@kias.re.kr

Published by the American Physical Society under the terms of the [Creative Commons Attribution 4.0 International license](https://creativecommons.org/licenses/by/4.0/). Further distribution of this work must maintain attribution to the author(s) and the published article’s title, journal citation, and DOI.

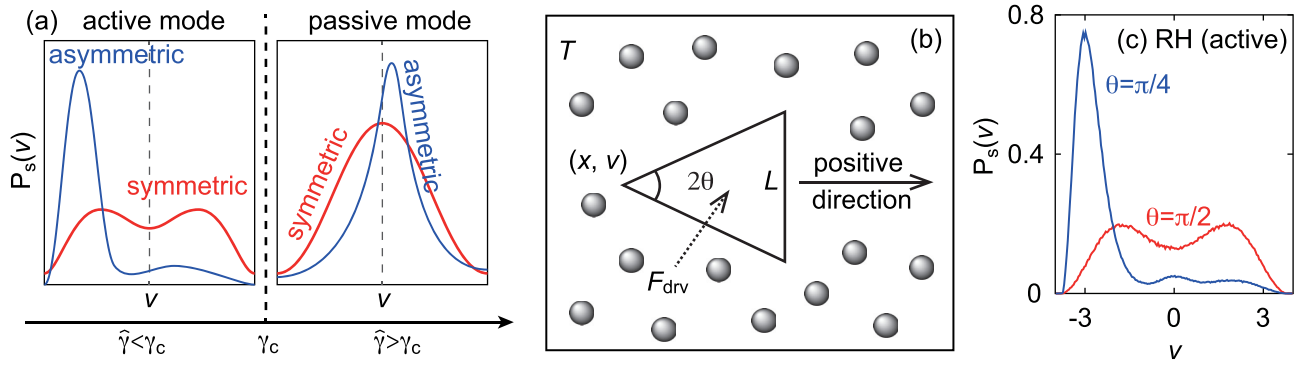


FIG. 1. (a) Schematic of the steady-state velocity distribution  $P_s(v)$  in one dimension for driving forces  $\mathbf{F}_{\text{drv}}$  in Eq. (1). When  $\hat{\gamma} < \gamma_c$  ( $\hat{\gamma} > \gamma_c$ ) with a symmetric particle shape, the velocity distribution is symmetric bimodal (unimodal) as shown by the left (right) red curve, which indicates the active (passive) mode. When the shape of a particle is asymmetric, one peak is amplified over the other for the active mode, while the peak position moves slightly aside with reduced variance for the passive mode (see the blue curves). (b) Schematic of the model. The  $t$  particle is immersed in a reservoir with temperature  $T$  and moves along the horizontal direction (one-dimensional motion). The reservoir consists of  $N$  identical  $r$  particles. The driving force  $F_{\text{drv}}$  is applied to the  $t$  particle. (c) The steady-state velocity distributions for the RH model in the active mode, obtained by numerical simulations. Those for other models and for the passive case are shown in Figs. S1 and S3 of the Supplemental Material [41].

reservoir of passive particles. This problem has been one of the important topics in the active-matter community, but a rigorous theoretical approach has not been addressed to date [36,37]. We find that the geometric asymmetry plays a crucial role for the rectified motion along with nonequilibriumness caused by  $\mathbf{F}_{\text{drv}}$ . We derive analytically the explicit formula for the rectified current and compare it with numerical results via extensive molecular dynamics simulations. Interestingly, a rectified current exists even in the passive mode, in particular, for  $\hat{\gamma} > 0$ , where the energy only dissipates (no energy pump-in). We coin the term “moving by dissipation” for this rectifying mechanism when  $\hat{\gamma} > 0$ . In practice, this type of rectification provides a weak but reliable (less dispersive) directed motion even in highly fluctuating thermal environments.

**Model.** Consider a triangular shaped particle ( $t$  particle) with mass  $M$  and vertical cross section  $L$  immersed in a reservoir with temperature  $T$  as illustrated in Fig. 1(b). Here, we constrain the  $t$ -particle motion along the horizontal direction only, where its translational motion is essentially equivalent to a rotational motion in the setup for various experimental and theoretical studies [26,27,38,39]. Its apex angle, position, and velocity are denoted as  $2\theta$ ,  $x$ , and  $v$ , respectively. The reservoir consists of  $N$  identical circular shaped particles ( $r$  particles) with mass  $m$  and radius  $R$  which move inside a two-dimensional square box with side length  $l$  with periodic boundary conditions. We assume that  $m \ll M$  and  $R \ll L \ll l$ . The stochastic motion of the  $t$  particle is induced by elastic collisions with  $r$  particles, which are equipped with the Langevin thermostat. Details of the collision dynamics and its numerical implementation [24,40] are described in the Supplemental Material [41]. Note that our analysis can be straightforwardly extended to an arbitrary convex shape.

Without any driving force, the  $t$  particle reaches a thermal equilibrium with zero mean velocity. However, with a one-dimensional force in Eq. (1) applied on the  $t$  particle, the system can be driven out of equilibrium. The resulting phenomena due to the driving forces are briefly summarized

in Fig. 1(a). The asymmetric shape of the  $t$  particle in the active mode breaks the symmetry of the peaks as shown by the left blue curve of Fig. 1(a); thus the active motion is rectified with a nonzero average current. This leads to the “rectified run-and-tumble” trajectory for the asymmetric active particle as shown by the blue lines in Fig. S2 of the Supplemental Material [41]. In the passive mode, the asymmetric shape of the  $t$  particle moves the position of the unimodal peak slightly aside, representing a *weak* rectified current compared with that in the active mode as shown by the right blue curve of Fig. 1(a).

**Theoretical analysis of the model.** To understand the emergence of the nonzero current analytically, we present a perturbation theory for the  $t$  particle dynamics for small  $m/M$ , which is reasonable in realistic situations. We also assume that  $r$  particles are always in equilibrium. Then, our model can be described by the kinetic theory introduced in Refs. [24,25] with the addition of an external driving force.

The probability density of the  $t$  particle velocity  $v$  at time  $t$ ,  $P(v, t)$ , can be described by the following Boltzmann master equation:

$$\frac{\partial P(v, t)}{\partial t} = (\mathcal{L}_{\text{res}} + \mathcal{L}_{\text{drv}})P(v, t), \quad (2)$$

where  $\mathcal{L}_{\text{res}}$  and  $\mathcal{L}_{\text{drv}}$  are operators representing the effects of the reservoir and the driving force, respectively. More specifically,  $\mathcal{L}_{\text{res}}$  can be written as

$$\mathcal{L}_{\text{res}} = \sum_{n=1}^{\infty} \frac{(-1)^n}{n!} \frac{\partial^n}{\partial v^n} a_n(v), \quad (3)$$

where a Kramers-Moyal coefficient  $a_n(v)$  is defined as  $a_n(v) \equiv \int r^n W(v+r|v)dr$  with the transition rate  $W(v'|v)$  from  $v$  to  $v'$  induced by elastic collisions with  $r$  particles [25,42,43]. The explicit calculation of  $a_n(v)$  is presented in Sec. II of the Supplemental Material [41].  $\mathcal{L}_{\text{drv}}$  is given by

$$\mathcal{L}_{\text{drv}} = -\frac{\partial}{\partial v} \frac{F_{\text{drv}}}{M}, \quad (4)$$

with  $F_{\text{drv}} = -\Gamma(v)v$  in Eq. (1).

It is convenient to introduce dimensionless variables

$$v \equiv v/v_0 \quad (v_0 \equiv \sqrt{k_B T/M}) \quad \text{and} \quad \tau = \gamma t/M, \quad (5)$$

where the t particle friction coefficient  $\gamma$  is obtained as

$$\gamma \equiv 4L\rho\sqrt{\frac{mk_B T}{2\pi}}(1 + \sin\theta), \quad (6)$$

with the r particle density  $\rho = N/l^2$  (see Sec. II of the Supplemental Material [41]). Then, Eq. (2) is rewritten as

$$\frac{\partial P(v, \tau)}{\partial \tau} = \sum_{n=1}^{\infty} \frac{(-1)^n}{n!} \frac{\partial^n}{\partial v^n} A_n(v) P(v, \tau), \quad (7)$$

where  $A_n(v)$  is the modified Kramers-Moyal coefficient defined as

$$A_n(v) = \frac{M}{\gamma v_0^n} a_n(v_0 v) - G(v)v\delta_{n,1} \quad (8)$$

with  $P(v, \tau) = v_0 P(v, t)$  and  $G(v) = \Gamma(v_0 v)/\gamma$ .

We perform a perturbation expansion with the small parameter  $\epsilon \equiv \sqrt{m/M}$ . Up to  $O(\epsilon)$ , we find in Sec. II of the Supplemental Material [41]

$$\begin{aligned} A_1(v) &\approx -[1 + G(v)]v + \bar{a}(1 - v^2)\epsilon, \\ A_2(v) &\approx 2 + 6\bar{a}v\epsilon, \\ A_3(v) &\approx -12\bar{a}\epsilon, \\ A_n(v) &= O(\epsilon^2), \quad \text{for } n \geq 4, \end{aligned} \quad (9)$$

where the asymmetric factor  $\bar{a} = \frac{\sqrt{2\pi}}{4}(1 - \sin\theta) \geq 0$ . Using Eqs. (7) and (9) and the expansion of  $P(v, \tau) \approx P^{(0)}(v, \tau) + \epsilon P^{(1)}(v, \tau)$ , we can set up the equations as follows:

$$\begin{aligned} \partial_\tau P^{(0)}(v, \tau) &= \mathcal{L}_0 P^{(0)}(v, \tau), \\ \partial_\tau P^{(1)}(v, \tau) &= \mathcal{L}_1 P^{(0)}(v, \tau) + \mathcal{L}_0 P^{(1)}(v, \tau), \end{aligned} \quad (10)$$

where  $\mathcal{L}_0$  and  $\mathcal{L}_1$  are given by

$$\begin{aligned} \mathcal{L}_0 &= -\frac{\partial}{\partial v} \left[ -[1 + G(v)]v - \frac{\partial}{\partial v} \right], \\ \mathcal{L}_1 &= -\bar{a} \frac{\partial}{\partial v} \left[ (1 - v^2) - 3 \frac{\partial}{\partial v} v - 2 \frac{\partial^2}{\partial v^2} \right]. \end{aligned} \quad (11)$$

The steady-state distribution of the zeroth order is then

$$P_s^{(0)}(v) = \frac{1}{\mathcal{N}} e^{-\int^v ds [1 + G(s)]s} \quad (12)$$

with the normalization factor  $\mathcal{N}$ . The next order is obtained by solving  $\mathcal{L}_0 P_s^{(1)}(v) = -\mathcal{L}_1 P_s^{(0)}(v)$ . A straightforward analysis yields

$$\begin{aligned} P_s^{(1)}(v) &= \bar{a} g(v) P_s^{(0)}(v) \quad \text{with} \\ g(v) &= 2G(v)v - \int_0^v ds G(s)[1 + 2G(s)]s^2. \end{aligned} \quad (13)$$

Note that  $g(v)$  is an odd function of  $v$ , i.e.,  $g(-v) = -g(v)$ , as  $G(v)$  is even in  $v$  in all models considered here. This is also consistent with the normalization condition  $\int_{-\infty}^{\infty} ds P_s^{(1)}(s) = 0$ .

The steady-state average of the  $n$ th moment of the velocity is then obtained up to  $O(\epsilon)$  as

$$\begin{aligned} \langle v^n \rangle_s &\approx \int_{-\infty}^{\infty} dv v^n [1 + \bar{a}\epsilon g(v)] P_s^{(0)}(v) \\ &= \begin{cases} \bar{a}\epsilon \langle v^n g(v) \rangle_0 & (n \text{ odd}) \\ \langle v^n \rangle_0 & (n \text{ even}), \end{cases} \end{aligned} \quad (14)$$

where  $\langle \dots \rangle_0$  stands for the average over  $P_s^{(0)}(v)$ . Note that the average velocity and its all-odd moments are  $O(\epsilon)$  and vanish for the symmetric case ( $\bar{a} = 0$ ). Thus the time-reversal symmetry breaking (rectified current) occurs only with a shape asymmetry and a finite mass ratio. All even moments responsible for the stochasticity are always  $O(1)$ , the same as that for  $\bar{a} = 0$ . The standard fluctuation is simply given by the second moment;  $\langle (\Delta v)^2 \rangle_s = \langle v^2 \rangle_s - \langle v \rangle_s^2 \approx \langle v^2 \rangle_0$ , up to  $O(\epsilon)$ . Equation (14) can be extended to a particle with arbitrary convex shape with the general expression of  $\bar{a}$  and  $\gamma$  (see Eqs. (S17) and (S22) in Secs. II and III of the Supplemental Material [41]). This indicates that the rectified motion is a general phenomenon for an active particle with asymmetric shape.

*Examples.* We first apply the analytic theory to a simple soluble example with  $F_{\text{drv}} = -\hat{\gamma}v$  to gain some insight. This model describes a ‘‘cold damping’’ problem applicable to a molecular refrigerator [44–46]. With Eqs. (12)–(14), we find

$$\langle v \rangle_s^{\text{sim}} = \bar{a}\epsilon \frac{\hat{\gamma}/\gamma}{(1 + \hat{\gamma}/\gamma)^2}, \quad \langle v^2 \rangle_s^{\text{sim}} = \frac{1}{1 + \hat{\gamma}/\gamma} \quad (15)$$

with  $P_s^{(0)}(v) \sim \exp[-(1 + \hat{\gamma}/\gamma)v^2/2]$  (see Sec. III of the Supplemental Material [41]). As expected, the rectification occurs as a result of the interplay of nonequilibrium driving ( $\hat{\gamma}$ ) and spatial asymmetry ( $\bar{a}$ ), even though the driving force does not favor any particular spatial direction. In this simple model, only the passive mode ( $\hat{\gamma} > -\gamma$ ) is allowed due to the dynamic instability in the active region. We get a nonzero current even when  $\hat{\gamma} > 0$  without energy input by the driving force. Thus this motion can be called ‘‘moving by dissipation’’ (mbd) denoting that unidirectional motion is induced by purely dissipative force. Note that the t particle can move in either direction, depending on the sign of  $\hat{\gamma}$ , and slows down for large positive  $\hat{\gamma}$ .

Now, we consider the more realistic models for active dynamics given by Eq. (1). We calculated the steady-state velocities  $\langle v \rangle_s^{\text{RH}}$ ,  $\langle v \rangle_s^{\text{dpt}}$ , and  $\langle v \rangle_s^{\text{SG}}$  and their fluctuations for the RH, the depot, and the SG models, respectively. The resulting expressions are rather complex and are presented in Sec. III of the Supplemental Material [41]. The velocities are plotted as solid curves in Fig. 2, which show that current amplitude is much bigger in the stabilized active mode ( $\hat{\gamma}/\gamma < -1$  for the RH and the depot models, and  $\hat{\gamma} < 0$  for the SG model) than in the passive mode. In fact,  $|\langle v \rangle_s|$  grows indefinitely as  $\hat{\gamma} \rightarrow -\infty$ , and its fluctuation also diverges. In the passive mode, we find a weaker positive current for the RH and the depot models as observed in the above simple example for  $\hat{\gamma} > 0$ . In contrast, the SG model shows an interesting crossover behavior from a positive to a negative current for positive  $\hat{\gamma}$  with  $\langle v \rangle_s^{\text{SG}} = -2\bar{a}\epsilon$  in the  $\hat{\gamma} \rightarrow \infty$  limit. Moreover, the fluctuation magnitude of the SG model decays faster than those of the other models:  $\langle v^2 \rangle_s \sim \hat{\gamma}^{-2}$  (SG) and  $\sim \hat{\gamma}^{-1}$  (RH and depot); see Sec. III and Fig. S8 of the Supplemental

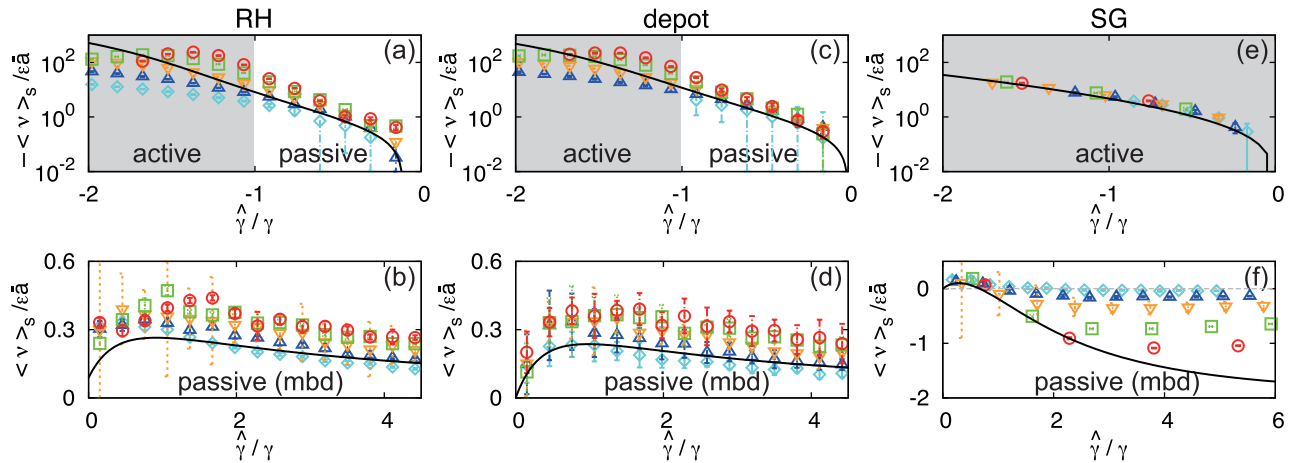


FIG. 2.  $\hat{\gamma}$  dependence of the rectified velocity. (a), (c), and (e) are the scaled steady-state velocities  $|\langle v \rangle_s|/(\bar{a}\epsilon)$  as a function of  $\hat{\gamma}/\gamma$  for the RH, the depot, and the SG models for negative  $\hat{\gamma}$ , respectively. (b), (d), and (f) are for positive  $\hat{\gamma}$ . Solid curves are analytic results. Cyan  $\diamond$ , blue  $\triangle$ , gold  $\nabla$ , green  $\square$ , and red  $\circ$  points denote data for  $M = 5, 10, 20, 50$ , and  $100$ , respectively, with  $m = 1$  fixed.

Material [41]. Thus the SG type would be more appropriate for designing reliable microscopic motors with both directional currents possible. As a reference, we estimate the order of magnitude of the rectification speed using realistic parameters of physical systems in Sec. IV of the Supplemental Material [41]. Note that this SG case was experimentally studied in Ref. [47].

*Numerical simulations.* To confirm the validity of our analysis, we performed extensive molecular dynamics simulations. Figure 1(c) shows numerical data for the steady-state velocity distributions of the  $t$  particle with a symmetric shape ( $\theta = \pi/2$ ) and an asymmetric shape ( $\theta = \pi/4$ ) in the active mode for the RH model. The rectification with broken symmetry is clearly seen in the figure. Similar distributions for the depot and the SG models are presented in Fig. S1 of the Supplemental Material [41]. The passive-mode velocity distributions with  $\theta = \pi/4$  and  $\hat{\gamma} > 0$  are presented in Fig. S3 of the Supplemental Material [41]; they are unimodal and slightly asymmetric as expected.

Data points in Fig. 2 are the simulation results for the rectified velocities of the asymmetric  $t$  particle with various values of  $\hat{\gamma}$  and  $t$ -particle mass  $M = 5, 10, 20, 50$ , and  $100$ . All other parameters are fixed (see the caption of Fig. S1 of the Supplemental Material [41]). We find that their overall behaviors agree well with the theoretical predictions qualitatively, but with  $\sim 40\%$  overestimates for the simple (Fig. S5 of the Supplemental Material [41]), the RH, and the depot models in the small- $\epsilon$  limit. The origin of this difference is unclear yet, but probably due to a reservoir finite-size effect, also noticed in previous studies in similar systems [24,25]. For the SG model, the numerical overestimate is much smaller, but the convergence to the small- $\epsilon$  limit is quite slow for large positive  $\hat{\gamma}/\gamma$ . This slow convergence is also found in the active mode for the RH and the depot models.

In addition to the emergence of the rectified current, we stress that the geometry-induced current is characterized by suppressed fluctuations in the mbd region. To highlight the usefulness of the mbd mechanism, we compare two simulated trajectories of the same  $t$  particle driven by either constant force ( $F_{\text{drv}} = f$ ) or the SG force. The two forces are tuned to

yield almost the same average velocity. The blue (red) curve in Fig. 3 is the trajectory averaged over 100 realizations when the  $t$  particle is driven by the constant (SG) force. The two trajectories have the same overall slope, but the trajectory from the constant force is much noisier. This strongly suggests that the mbd mechanism can be utilized as a motor mechanism when an accurate motion is required in highly fluctuating environments. However, the rectification speed is quite small as  $O(\epsilon)$  in the passive mode; thus its usefulness is rather limited. Note that the origin of the moving by dissipation, motion induced by a geometric asymmetry, is different from that in Refs. [48,49], motion induced by an asymmetric dissipative force.

*Conclusion and discussion.* Our study clearly demonstrates that the self-propelled motion of an active object can be rectified by its shape asymmetry in passive environments. Our conclusion is applicable to an active object with arbitrary convex shape, driven by a general velocity-dependent force induced by a symmetric velocity potential  $\Phi(v)$ . We also show that this rectification is possible even in the passive mode without a self-propelled velocity. Especially, for  $\hat{\gamma} > 0$ , the motion is driven by the mbd mechanism, which can provide a design principle for developing more reliable microscopic motors. We note that the active particle motion is also

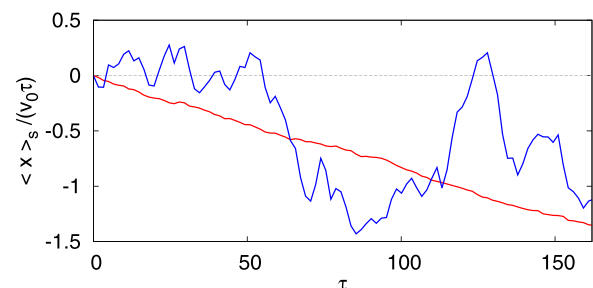


FIG. 3. Trajectories of the  $t$  particle averaged over 100 realizations driven by a constant force  $f = 5.1 \times 10^{-3} \gamma v_0$  (blue) and the SG force with  $\hat{\gamma}/\gamma = 9.88$  (red).  $\tau$  has a dimensionless time unit as defined in Eq. (5).

modeled by introducing a self-propulsion velocity through energy conversions by chemical fuels or reactions [7,50]. We find a similar rectification behavior by numerical simulations, shown in Fig. S6 of the Supplemental Material [41].

It is also imaginable that some microorganisms or nanomachines driven by chemical fuels make use of this rectification mechanism by changing their shape asymmetrically to move in an intended direction. Moreover, the magnitude and direction of the particle velocity can be controlled by simply changing its shape, i.e.,  $\theta$  as shown in Fig. S9 of the Supplemental Material [41]. This suggests that the shape change of microorganisms might have an important role in controlling their movement.

Finally, we remark that our result is restricted to one-dimensional motion but is still relevant to important problems such as a molecular motor walking along a microtubule, blood cell movement inside a capillary vessel, and a rotary molecu-

lar gear. In higher dimensions, the rectification will disappear eventually in the long-time limit due to a possible rotational diffusion, but may generate an intricate interplay between the rotation diffusive time scale and the rectification speed, which is left for future study.

## ACKNOWLEDGMENTS

The authors acknowledge the Korea Institute for Advanced Study for providing computing resources (KIAS Center for Advanced Computation Linux Cluster System). This research was supported by NRF Grants No. 2017R1D1A1B06035497 (H.P.) and No. 2019R1A2C1009628 (J.D.N.) and KIAS Individual Grants No. PG013604 (H.P.), No. PG074002 (J.-M.P.), and No. PG064901 (J.S.L.) at Korea Institute for Advanced Study.

- 
- [1] P. Romanczuk, M. Bär, W. Ebeling, B. Lindner, and L. Schimansky-Geier, Active Brownian particles. From individual to collective stochastic dynamics, *Eur. Phys. J.: Spec. Top.* **202**, 1 (2012).
  - [2] X.-L. Wu and A. Libchaber, Particle Diffusion in a Quasi-Two-Dimensional Bacterial Bath, *Phys. Rev. Lett.* **84**, 3017 (2000).
  - [3] K. C. Leptos, J. S. Guasto, J. P. Gollub, A. I. Pesci, and R. E. Goldstein, Dynamics of Enhanced Tracer Diffusion in Suspensions of Swimming Eukaryotic Microorganisms, *Phys. Rev. Lett.* **103**, 198103 (2009).
  - [4] J. Palacci, C. Cottin-Bizonne, C. Ybert, and L. Bocquet, Sedimentation and Effective Temperature of Active Colloidal Suspensions, *Phys. Rev. Lett.* **105**, 088304 (2010).
  - [5] H. Kurtuldu, J. S. Guasto, K. A. Johnson, and J. P. Gollub, Enhancement of biomixing by swimming algal cells in two-dimensional films, *Proc. Natl. Acad. Sci. USA* **108**, 10391 (2011).
  - [6] C. Maggi, M. Paoluzzi, N. Pellicciotta, A. Lepore, L. Angelani, and R. Di Leonardo, Generalized Energy Equipartition in Harmonic Oscillators Driven by Active Baths, *Phys. Rev. Lett.* **113**, 238303 (2014).
  - [7] Y. Fily and M. C. Marchetti, Athermal Phase Separation of Self-Propelled Particles with No Alignment, *Phys. Rev. Lett.* **108**, 235702 (2012).
  - [8] S. Krishnamurthy, S. Ghosh, D. Chatterji, R. Ganapathy, and A. K. Sood, A micrometre-sized heat engine operating between bacterial reservoirs, *Nat. Phys.* **12**, 1134 (2016).
  - [9] R. Zakine, A. Solon, T. Gingrich, and F. van Wijland, Stochastic Stirling engine operating in contact with active baths, *Entropy* **19**, 193 (2017).
  - [10] J. S. Lee, J.-M. Park, and H. Park, Brownian heat engine with active reservoirs, *Phys. Rev. E* **102**, 032116 (2020).
  - [11] C. Kwon, J. Yeo, H. K. Lee, and H. Park, Unconventional entropy production in the presence of momentum-dependent forces, *J. Korean Phys. Soc.* **68**, 633 (2016).
  - [12] H. K. Lee, S. Lahiri, and H. Park, Nonequilibrium steady states in Langevin thermal systems, *Phys. Rev. E* **96**, 022134 (2017).
  - [13] É. Fodor, C. Nardini, M. E. Cates, J. Tailleur, P. Visco, and F. van Wijland, How Far from Equilibrium Is Active Matter? *Phys. Rev. Lett.* **117**, 038103 (2016).
  - [14] L. Dabelow, S. Bo, and R. Eichhorn, Irreversibility in Active Matter Systems: Fluctuation Theorem and Mutual Information, *Phys. Rev. X* **9**, 021009 (2019).
  - [15] M. Badoual, F. Jülicher, and J. Prost, Bidirectional cooperative motion of molecular motors, *Proc. Natl. Acad. Sci. USA* **99**, 6696 (2002).
  - [16] D. Chaudhuri, Active Brownian particles: Entropy production and fluctuation response, *Phys. Rev. E* **90**, 022131 (2014).
  - [17] C. Ganguly and D. Chaudhuri, Stochastic thermodynamics of active Brownian particles, *Phys. Rev. E* **88**, 032102 (2013).
  - [18] F. Schweitzer, W. Ebeling, and B. Tilch, Complex Motion of Brownian Particles with Energy Depots, *Phys. Rev. Lett.* **80**, 5044 (1998).
  - [19] W. Ebeling, F. Schweitzer, and B. Tilch, Active Brownian particles with energy depots modeling animal mobility, *BioSystems* **49**, 17 (1999).
  - [20] C. A. Condat, and G. J. Sibona, Diffusion in a model for active Brownian motion, *Phys. D (Amsterdam)* **168**, 235 (2002).
  - [21] V. Garcia, M. Birbaumer, and F. Schweitzer, Testing an agent-based model of bacterial cell motility: How nutrient concentration affects speed distribution, *Eur. Phys. J. B* **82**, 235 (2011).
  - [22] M. Schienbein and H. Gruler, Langevin equation, Fokker-Planck equation and cell migration, *Bull. Math. Biol.* **55**, 585 (1993).
  - [23] U. Erdmann, W. Ebeling, L. Schimansky-Geier, and F. Schweitzer, Brownian particles far from equilibrium, *Eur. Phys. J. B* **15**, 105 (2000).
  - [24] C. Van den Broeck, R. Kawai, and P. Meurs, Microscopic Analysis of a Thermal Brownian Motor, *Phys. Rev. Lett.* **93**, 090601 (2004).
  - [25] P. Meurs, C. Van den Broeck, and A. Garcia, Rectification of thermal fluctuations in ideal gases, *Phys. Rev. E* **70**, 051109 (2004).
  - [26] A. Sokolov, M. M. Apodaca, B. A. Grzybowski, and I. S. Aranson, Swimming bacteria power microscopic gears, *Proc. Natl. Acad. Sci. USA* **107**, 969 (2010).
  - [27] R. Di Leonardo, L. Angelani, D. Dell'Arciprete, G. Ruocco, V. Iebba, S. Schippa, M. P. Conte, F. Mecarini, F. De Angelis, and

- E. Di Fabrizio, Bacterial ratchet motors, *Proc. Natl. Acad. Sci. USA* **107**, 9541 (2010).
- [28] L. Angelani, R. Di Leonardo, and G. Ruocco, Self-Starting Micromotors in a Bacterial Bath, *Phys. Rev. Lett.* **102**, 048104 (2009).
- [29] Y. Baek, A. P. Solon, X. Xu, N. Nikola, and Y. Kafri, Generic Long-Range Interactions Between Passive Bodies in an Active Fluid, *Phys. Rev. Lett.* **120**, 058002 (2018).
- [30] L. Angelani and R. Di Leonardo, Geometrically biased random walks in bacteria-driven micro-shuttles, *New J. Phys.* **12**, 113017 (2010).
- [31] A. Kaiser, A. Peshkov, A. Sokolov, B. ten Hagen, H. Löwen, and I. S. Aranson, Transport Powered by Bacterial Turbulence, *Phys. Rev. Lett.* **112**, 158101 (2014).
- [32] N. Nikola, A. P. Solon, Y. Kafri, M. Kardar, J. Tailleur, and R. Voituriez, Active Particles with Soft and Curved Walls: Equation of State, Ratchets, and Instabilities, *Phys. Rev. Lett.* **117**, 098001 (2016).
- [33] C. J. O. Reichhardt and C. Reichhardt, Ratchet effects in active matter systems, *Annu. Rev. Condens. Matter Phys.* **8**, 51 (2017).
- [34] G. Vizsnyiczai, G. Frangipane, C. Maggi, F. Saglimbeni, S. Bianchi, and R. Di Leonardo, Light controlled 3D micromotors powered by bacteria, *Nat. Commun.* **8**, 15974 (2017).
- [35] A. Kaiser, A. Sokolov, I. S. Aranson, and H. Löwen, Motion of two micro-wedges in a turbulent bacterial bath, *Eur. Phys. J.: Spec. Top.* **224**, 1275 (2015).
- [36] A. Aubret, M. Youssef, S. Sacanna, and J. Palacci, Targeted assembly and synchronization of self-spinning microgears, *Nat. Phys.* **14**, 1114 (2018).
- [37] F. Kümmel, B. ten Hagen, R. Wittkowski, I. Buttinoni, R. Eichhorn, G. Volpe, H. Löwen, and C. Bechinger, Circular Motion of Asymmetric Self-Propelling Particles, *Phys. Rev. Lett.* **110**, 198302 (2013).
- [38] C. Van den Broeck and R. Kawai, Brownian Refrigerator, *Phys. Rev. Lett.* **96**, 210601 (2006).
- [39] M. van den Broeck and C. Van den Broeck, Chiral Brownian Heat Pump, *Phys. Rev. Lett.* **100**, 130601 (2008).
- [40] J. S. Lee and H. Park, Additivity of multiple heat reservoirs in the Langevin equation, *Phys. Rev. E* **97**, 062135 (2018).
- [41] See Supplemental Material at <http://link.aps.org/supplemental/10.1103/PhysRevResearch.3.L042011> for details of numerical simulations and analytic derivations.
- [42] H. Risken, *The Fokker-Planck Equation* (Springer, Berlin, 1989).
- [43] N. G. van Kampen, *Stochastic Processes in Physics and Chemistry* (Elsevier, New York, 2007).
- [44] M. Pinard, P. F. Cohadon, T. Briant, and A. Heidmann, Full mechanical characterization of a cold damped mirror, *Phys. Rev. A* **63**, 013808 (2000).
- [45] K. H. Kim and H. Qian, Entropy Production of Brownian Macromolecules with Inertia, *Phys. Rev. Lett.* **93**, 120602 (2004).
- [46] G. Jourdan, G. Torricelli, J. Chevrier, and F. Comin, Tuning the effective coupling of an AFM lever to a thermal bath, *Nanotechnology* **18**, 475502 (2007).
- [47] A. Gnoli, A. Petri, F. Dalton, G. Gradenigo, A. Sarracino, and A. Puglisi, Brownian Ratchet in a Thermal Bath Driven by Coulomb Friction, *Phys. Rev. Lett.* **110**, 120601 (2013).
- [48] J. Talbot, R. D. Wildman, and P. Viot, Kinetics of a Frictional Granular Motor, *Phys. Rev. Lett.* **107**, 138001 (2011).
- [49] R. García-García, P. Collet, and L. Truskinovsky, Guided active particles, *Phys. Rev. E* **100**, 042608 (2019).
- [50] S. J. Ebbens and J. R. Howse, In pursuit of propulsion at the nanoscale, *Soft Matter* **6**, 726 (2010).

**Supplementary Material for**  
**“Geometry-induced rectification for an active object”**

Jae Sung Lee<sup>1,\*</sup>, Jong-Min Park<sup>1</sup>, Jae Dong Noh<sup>2</sup>, and Hyunggyu Park<sup>1†</sup>

<sup>1</sup>*School of Physics, Korea Institute for Advanced Study, Seoul 02455, Korea and*

<sup>2</sup> *Department of Physics, University of Seoul, Seoul 02504, Korea*

---

\* jslee@kias.re.kr

† hgpark@kias.re.kr

## I. MOLECULAR DYNAMICS SIMULATIONS

We consider a triangular shaped particle (t-particle) with mass  $M$  in a reservoir with  $N$  identical circular reservoir particles (r-particles) as shown in Fig. 1 (b) of the main text. The t-particle moves only in the horizontal direction, while the r-particles move inside the two-dimensional box with periodic boundary conditions. Interactions between the r-particles are modeled as hard-disk elastic collisions. For convenience, an elastic collision between a r-particle and the t-particle is assumed to occur when the r-particle center touches the boundary of the t-particle [1, 2].

We adopt the Langevin thermostat to maintain the reservoir temperature  $T$  [3]. Thus, the equation of motion of the  $i$ -th r-particle ( $i = 1, \dots, N$ ) is given by [2]

$$\mathbf{v}_i = \dot{\mathbf{x}}_i, \quad m\dot{\mathbf{v}}_i = \mathbf{F}_i^{\text{col}} - \gamma_{\text{th}}\mathbf{v}_i + \boldsymbol{\xi}_i, \quad (\text{S1})$$

where  $\mathbf{x}_i$  and  $\mathbf{v}_i$  are the two-dimensional position and velocity vectors of the  $i$ -th r-particle, respectively,  $\gamma_{\text{th}}$  is the dissipation coefficient for the thermostat, and  $\mathbf{F}_i^{\text{col}}$  describes the interaction force induced by collisions with the t-particle and other r-particles.  $\boldsymbol{\xi}_i$  is the Gaussian white noise vector satisfying  $\langle \boldsymbol{\xi}_i(t)\boldsymbol{\xi}_j^\top(t') \rangle = 2\gamma_{\text{th}}k_{\text{B}}T\delta_{ij}\delta(t-t')\mathbb{I}$ , where  $\mathbb{I}$  is the  $N \times N$  identity matrix and  $k_{\text{B}}$  is the Boltzmann constant.

The t-particle motion is affected by the elastic collisions with r-particles and also by the driving force in Eq. (1) of the main text. As we constrain the t-particle motion in one dimension (horizontal direction), the equation of motion of the t-particle is

$$v = \dot{x}, \quad M\dot{v} = -\mathbf{F}_x^{\text{col}} + F_{\text{drv}}, \quad (\text{S2})$$

where  $x$  and  $v$  are the position and the velocity of the t-particle,  $\mathbf{F}_x^{\text{col}}$  is the horizontal component of the total collision force ( $\mathbf{F}^{\text{col}} = \sum_i \mathbf{F}_i^{\text{col}}$ ), and the one-dimensional driving force  $F_{\text{drv}} = -\Gamma(v)v$ .

For numerical simulations, we set the parameter values as  $l = 300$ ,  $N = 200$ ,  $k_{\text{B}}T = 4$ ,  $R = 0.5$ ,  $L = 4$ ,  $\gamma_{\text{th}} = 1$ ,  $m = 1$ ,  $\omega = 0.01$ , and  $\zeta = 0.2$ . The apex angle  $\theta = \pi/2$  is taken for the symmetric shape (vertical rod) and  $\theta = \pi/4$  for a typical asymmetric shape. We vary  $\hat{\gamma}$  and  $M$  to investigate the dependence on the driving force strength ( $\hat{\gamma}$ ) and also on the mass ratio ( $m/M$ ). By solving the equations of motion in Eqs. (S1) and (S2) numerically with kinematic considerations for all involved collisions, we generate numerical data for the



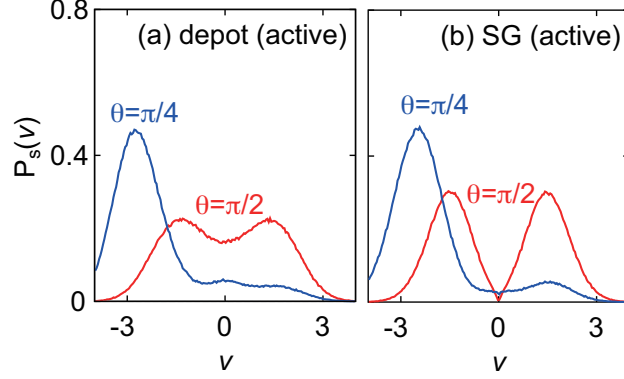


FIG. S1. The steady-state velocity distributions for (a) the depot and (b) the SG models in the active mode. Red and blue curves are plots for  $\theta = \pi/2$  (symmetric) and  $\pi/4$  (asymmetric), respectively. All distributions including Fig. 1(c) of the main text are obtained from numerical simulations with parameter values of  $l = 300$ ,  $N = 200$ ,  $k_B T = 4$ ,  $R = 0.5$ ,  $L = 4$ ,  $\gamma_{\text{th}} = 1$ ,  $m = 1$ ,  $M = 20$ ,  $\hat{\gamma} = -0.14$ ,  $\omega = 0.01$ , and  $\zeta = 0.2$ . To obtain these distributions, we averaged over  $8 \times 10^5$  velocity data from  $10^4$  trajectories in the steady state; 80 data are taken from each trajectory with the time interval  $\Delta t = 500 > M/\gamma \simeq 300$ .

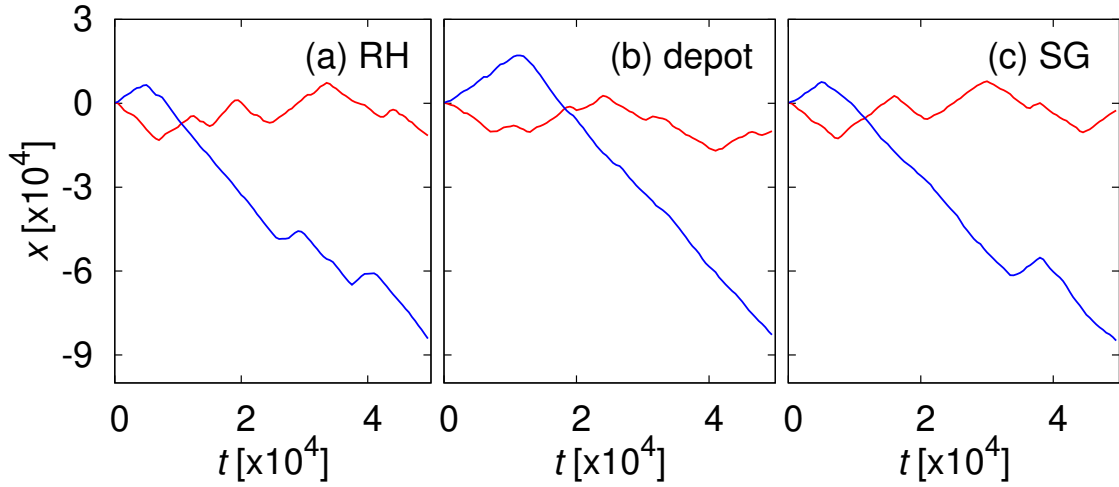


FIG. S2. (a), (b), and (c) are trajectories of the t-particle in the active mode of the RH, the depot, and the SG models, respectively. Red and blue curves denote trajectories for the symmetric ( $\theta = \pi/2$ ) and the asymmetric ( $\theta = \pi/4$ ) case, respectively. The symmetric-shaped particle shows a usual run-and-tumble motion with zero-mean velocity, while the asymmetric-shaped particle shows a rectified run-and-tumble motion.

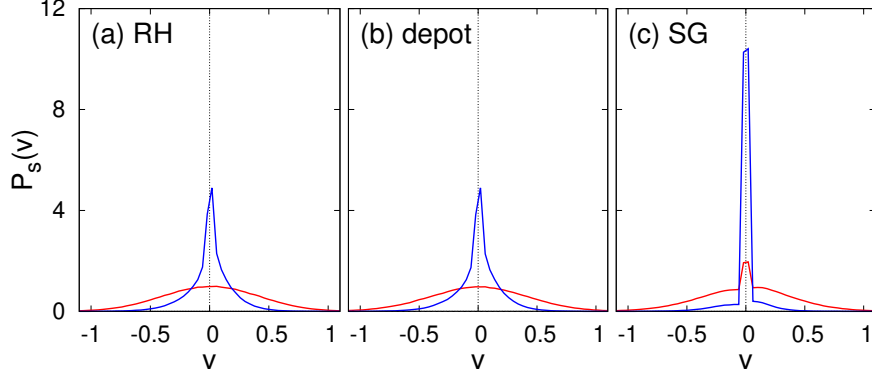


FIG. S3. The steady-state velocity distribution for (a) the RH, (b) the depot, and (c) the SG models in the passive mode with positive  $\hat{\gamma}$ . We take  $\hat{\gamma}/\gamma = 0.152$  (red) and  $\hat{\gamma}/\gamma = 4.42$  (blue) for the RH and the depot models, and  $\hat{\gamma}/\gamma = 0.341$  (red) and  $\hat{\gamma}/\gamma = 9.88$  (blue) for the SG model. The distributions are unimodal with weak asymmetry.

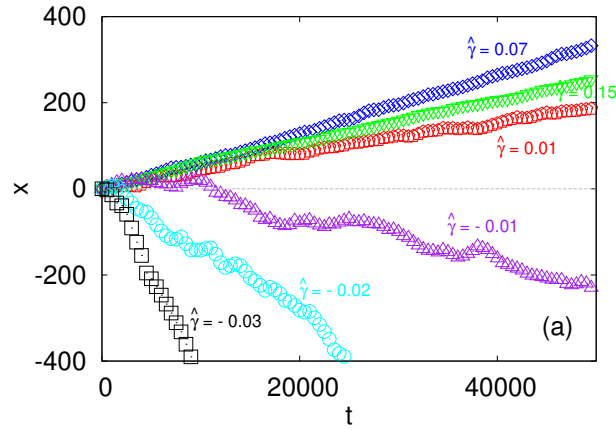


FIG. S4. Trajectories of the  $t$ -particle averaged over 5000 realizations for various values of  $\hat{\gamma}$  for the simple model with  $F_{\text{drv}} = -\hat{\gamma}v$ .

$t$ -particle trajectories in the phase space of  $(x, v)$ . After discarding initial transient data before  $t = 10M/\gamma$ , we calculate the steady-state velocity distribution  $P_s(v)$  as well as its first and second moments, i.e.  $\langle v \rangle_s$  and  $\langle v^2 \rangle_s$ .

With  $\hat{\gamma} = -0.14$  and  $M = 20$ , the numerically obtained  $P_s(v)$  are plotted in Fig. 1(c) of the main text and in Fig. S1 both for the symmetric and the asymmetric cases in the active mode of the three different models. Typical run-and-tumble trajectories of the  $t$ -particle are shown in Fig. S2. We also present numerical data in the passive mode with  $\hat{\gamma} > 0$  in Fig. S3.

The averaged trajectories for the simple model ( $F_{\text{drv}} = -\hat{\gamma}v$ ) are shown for various values

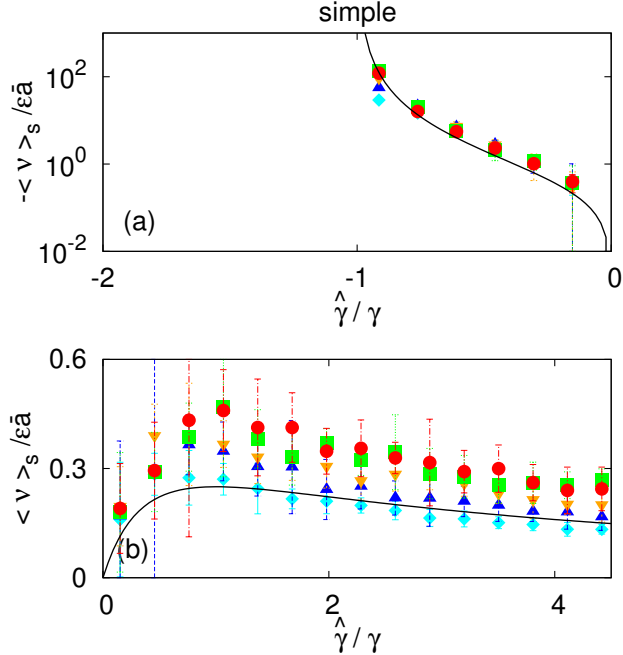


FIG. S5. The scaled steady-state velocities  $\langle \nu \rangle_s / (\bar{a}\epsilon)$  as a function of  $\hat{\gamma}/\gamma$  for the simple model (a) for  $\hat{\gamma} < 0$  and (b) for  $\hat{\gamma} > 0$ . Solid curves are analytic results. Cyan  $\diamond$ , blue  $\triangle$ , gold  $\nabla$ , green  $\square$ , red  $\circ$  points denote data for  $M = 5, 10, 20, 50,$  and  $100$ , respectively.

of  $\hat{\gamma}$  in Fig. S4, which are qualitatively consistent with Eq. (15) of the main text.

We measure the average velocities of the asymmetric t-particle for the simple, the RH, the depot, and the SG model for various  $\hat{\gamma}$  ranging from  $-0.13$  to  $+0.29$  with the t-particle mass  $M = 5, 10, 20, 50, 100$ , which are plotted in Fig. S5 and Fig. 2 of the main text. For convenience, we use the scaled axes of  $\hat{\gamma}/\gamma$  and  $\langle \nu \rangle_s / (\bar{a}\epsilon)$ . We note that the t-particle friction coefficient  $\gamma$  is obtained numerically by measuring the diffusion of the t-particle without a driving force and using the Einstein relation  $\gamma = k_B T / D$  with the steady-state position fluctuation  $\langle (\Delta x)^2 \rangle_s = 2Dt$  [4, 5]. The result is  $\gamma \approx 0.067$ .

We also consider a driving force  $F_{\text{drv}} = \gamma v_{\text{self}} \cos \phi$  with a fluctuating variable  $\phi(t)$ , satisfying the dynamic equation of  $\dot{\phi} = \eta$  with a Gaussian white noise  $\eta(t)$  where  $\langle \eta(t) \rangle = 0$  and  $\langle \eta(t)\eta(t') \rangle = 2D_\phi \delta(t - t')$ . This case corresponds to a one-dimensional version of the active Brownian particle dynamics with a constant speed  $v_{\text{self}}$  and diffusive angular motion [6, 7]. In this model, nonequilibrium activeness is given by finite  $v_{\text{self}} (\geq 0)$ . The numerical data for the average velocity are plotted against  $v_{\text{self}}$  in Fig. S6, which are similar to the results for three other models in the active mode, i.e. negative velocity increasing with the activity

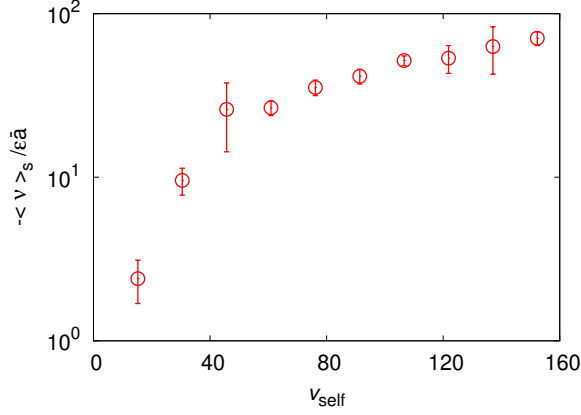


FIG. S6. The scaled average velocity versus  $v_{\text{self}}$  for the one-dimensional version of the active Brownian particle model with  $D_\phi = 1$ .

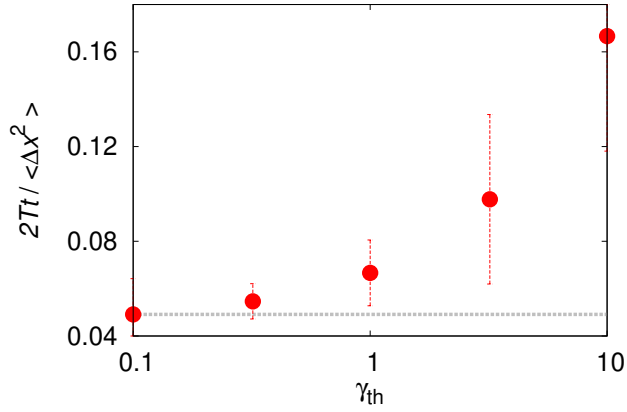


FIG. S7.  $\gamma_{\text{th}}$ -dependence of  $\gamma$ . The gray dotted line denotes the theoretical value of  $\gamma$  directly calculated from Eq. (6) of the main text.

strength.

*$\gamma_{\text{th}}$ -dependence of  $\gamma$*  – The friction coefficient  $\gamma$  was derived analytically in SM II and given as  $\gamma = 4L\rho\sqrt{mk_{\text{B}}T/(2\pi)}(1 + \sin\theta)$  in Eq. (6) of the main text. Note that this result does not depend on the thermostat dissipation coefficient  $\gamma_{\text{th}}$ , as it should be with an *ideal* heat reservoir with a high Knudsen number, no sound wave effect, and so on. However, in molecular dynamic simulations, the reservoir effect is modeled by kinematic collisions with a finite number of reservoir particles with a Langevin thermostat in a finite box, which causes a spurious  $\gamma_{\text{th}}$ -dependence [2].

Simulation results with  $M = 20$  and  $\hat{\gamma} = 0$  are plotted in Fig. S7 by estimating  $\gamma$  through

measuring the position fluctuation and using the Einstein relation, i.e.  $\gamma = 2k_B T t / \langle \Delta x^2 \rangle_s$ . It clearly depends on and increases with  $\gamma_{\text{th}}$ . The theoretical value for the given set of parameters is  $\gamma \simeq 0.0484$ . Interestingly, one can see that the numerical estimate approaches the theoretical value for small  $\gamma_{\text{th}}$ . With  $\gamma_{\text{th}} = 1$  (used in most of our simulations), we find  $\gamma \approx 0.067$  which is  $\sim 40\%$  bigger than the theoretical value. One may ascribe this overestimate to an effectively higher r-particle density  $\rho$  near the t-particle for large  $\gamma_{\text{th}}$ . After colliding with the t-particle, a r-particle tends to move away but its velocity distribution relaxes back to equilibrium quickly with large  $\gamma_{\text{th}}$  (smaller relaxation time). This makes a little higher r-particle density near the t-particle, compared to a smaller  $\gamma_{\text{th}}$  case. With a higher effective  $\rho$ , one can expect a bigger  $\gamma$  from the above theoretical formula.

## II. KRAMERS-MOYAL COEFFICIENTS

The Kramers-Moyal coefficients  $\{a_n(v)\}$  (“jump moments”) for a single object with an arbitrary convex shape in an ideal heat reservoir were derived in [1, 8]. We first show this derivation briefly here for completeness.

Consider a collision event of a r-particle with velocity  $\mathbf{v}_r$  with the Brownian object (t-particle) with velocity  $v$  on its surface point parametrized by the orientation angle  $\phi$  measured from the horizontal ( $x$ ) axis. After this collision, the t-particle will take the post-collision velocity  $v_\phi(v, \mathbf{v}_r)$  determined by the given kinematics. Then, the transition rate of the t-particle velocity from  $v$  to  $v'$  is given as

$$W(v'|v) = \int d\phi d^2\mathbf{v}_r \delta(v' - v_\phi(v, \mathbf{v}_r)) w_\phi(v, \mathbf{v}_r) P(\mathbf{v}_r), \quad (\text{S3})$$

where  $P(\mathbf{v}_r)$  is the equilibrium velocity distribution of r-particles,  $w_\phi(v, \mathbf{v}_r)$  is the rate of such a collision event, and  $\delta$  is the Dirac delta function. We assume that the r-particles are always in thermal equilibrium with temperature  $T$  (ideal reservoir), regardless of collision events, leading to the Maxwellian velocity distribution as

$$P(\mathbf{v}_r) = \frac{m}{2\pi k_B T} \exp\left(-\frac{m}{2k_B T} |\mathbf{v}_r|^2\right). \quad (\text{S4})$$

The collision rate  $w_\phi(v, \mathbf{v}_r)$  can be obtained by the product of the collision cross section and the incoming r-particle flux rate normal to the collision surface. The cross section can be written as  $S F_\phi$  with the total circumference of the t-particle surface  $S$  and its angular

fraction  $F_\phi$  (“form factor”). For the triangular shape here, we can easily find

$$\begin{aligned} S &= L + \frac{L}{\sin \theta}, \\ F_\phi &= \frac{L}{S} \delta(\phi - \frac{\pi}{2}) + \frac{L}{2S \sin \theta} \delta(\phi - \pi - \theta) + \frac{L}{2S \sin \theta} \delta(\phi - 2\pi + \theta). \end{aligned} \quad (\text{S5})$$

Meanwhile, the particle flux rate is determined by the normal component of the relative velocity of two particles times the r-particle density. Thus, the collision rate can be written as

$$w_\phi(v, \mathbf{v}_r) = SF_\phi \rho |(v\hat{\mathbf{e}}_x - \mathbf{v}_r) \cdot \hat{\mathbf{e}}_{\phi\perp}| H((v\hat{\mathbf{e}}_x - \mathbf{v}_r) \cdot \hat{\mathbf{e}}_{\phi\perp}) \quad (\text{S6})$$

with the r-particle density  $\rho$ , the unit vectors  $\hat{\mathbf{e}}_x(\hat{\mathbf{e}}_y)$  of the  $x(y)$  axis, and the unit vector  $\hat{\mathbf{e}}_{\phi\perp} = (\sin \phi)\hat{\mathbf{e}}_x - (\cos \phi)\hat{\mathbf{e}}_y$  normal to the surface. The Heaviside step function  $H(x)$  guarantees a collision by excluding the outgoing flux:  $H(x) = 1$  for  $x > 0$ , and 0 for  $x < 0$ .

The post-collision velocity  $v_\phi(v, \mathbf{v}_r)$  of the t-particle is determined by the elastic kinematics, such that the kinetic energy and the  $x$ -component momentum are conserved, while the  $y$ -component momentum is not conserved due to the constraint of the t-particle motion only in the  $x$  direction. Instead, by assuming only the normal force reacting on the colliding r-particle, the r-particle momentum parallel to the surface is conserved. These three conservation laws read

$$\begin{aligned} \frac{1}{2}Mv^2 + \frac{1}{2}m|\mathbf{v}_r|^2 &= \frac{1}{2}Mv_\phi^2 + \frac{1}{2}m|\mathbf{v}'_r|^2, \\ Mv + m\mathbf{v}_r \cdot \hat{\mathbf{e}}_x &= Mv_\phi + m\mathbf{v}'_r \cdot \hat{\mathbf{e}}_x, \\ m\mathbf{v}_r \cdot \hat{\mathbf{e}}_{\phi\parallel} &= m\mathbf{v}'_r \cdot \hat{\mathbf{e}}_{\phi\parallel}, \end{aligned} \quad (\text{S7})$$

where  $\mathbf{v}'_r$  is the post-collision velocity of the r-particle and  $\hat{\mathbf{e}}_{\phi\parallel} = (\cos \phi)\hat{\mathbf{e}}_x + (\sin \phi)\hat{\mathbf{e}}_y$  is the unit vector parallel to the surface with the orientation angle  $\phi$ . It is straightforward to find the solution for  $v_\phi$  as

$$v_\phi(v, \mathbf{v}_r) = v + (\mathbf{v}_r \cdot \hat{\mathbf{e}}_x - v - \mathbf{v}_r \cdot \hat{\mathbf{e}}_y \cot \phi) / \beta, \quad (\text{S8})$$

where  $\beta = (1 + \epsilon^2 \sin^2 \phi) / (2\epsilon^2 \sin^2 \phi)$  with  $\epsilon = \sqrt{m/M}$ .

By inserting Eqs. (S4), (S6), and (S8) into Eq. (S3) and integrating it over  $\mathbf{v}_r$ , we find

$$W(v + r|v) = -Spr \int d\phi F(\phi) H(-r \sin \phi) \sqrt{\frac{\alpha^2}{\pi}} \beta^2 \sin \phi \exp(-\alpha^2 (v + \beta r)^2) \quad (\text{S9})$$

with the jump amplitude  $r$  ( $v' = v + r$ ) and  $\alpha = \sqrt{m/2k_B T} \sin \phi$ . The Kramers-Moyal coefficients  $a_n(v)$  defined in Eq. (3) of the main text is then split into two parts

$$a_n(v) = S\rho \sqrt{\frac{2k_B T}{\pi m}} \left( - \int_{-\infty}^0 dr \int_{\alpha>0} d\phi + \int_0^{\infty} dr \int_{\alpha<0} d\phi \right) F(\phi) \alpha^2 \beta^2 r^{n+1} e^{-\alpha^2(v+\beta r)^2}. \quad (\text{S10})$$

Using the following integral formula

$$\begin{aligned} & a^2 b^2 \int_0^{\infty} dr r^{n+1} e^{-a^2(v+br)^2} \\ &= \frac{e^{-a^2 v^2}}{2|ab|^n} \left[ \Gamma\left(1 + \frac{n}{2}\right) \Phi\left(1 + \frac{n}{2}, \frac{1}{2}, a^2 v^2\right) - 2v \frac{|ab|}{b} \Gamma\left(\frac{3+n}{2}\right) \Phi\left(\frac{3+n}{2}, \frac{3}{2}, a^2 v^2\right) \right], \end{aligned} \quad (\text{S11})$$

we finally obtain

$$\begin{aligned} a_n(v) = & S\rho \int d\phi F(\phi) \frac{1}{2} \sqrt{\frac{2k_B T}{\pi m}} (-\alpha\beta)^{-n} e^{-\alpha^2 v^2} \\ & \times \left[ \Gamma\left(1 + \frac{n}{2}\right) \Phi\left(1 + \frac{n}{2}, \frac{1}{2}, \alpha^2 v^2\right) + 2\alpha v \Gamma\left(\frac{3+n}{2}\right) \Phi\left(\frac{3+n}{2}, \frac{3}{2}, \alpha^2 v^2\right) \right] \end{aligned} \quad (\text{S12})$$

with the Gamma function

$$\Gamma(z) = \int_0^{\infty} dx x^{z-1} e^{-x} \quad (\text{S13})$$

and the Kummer's function

$$\Phi(a, b, z) = \frac{\Gamma(b)}{\Gamma(b-a)\Gamma(a)} \int_0^1 dt e^{zt} t^{a-1} (1-t)^{b-a-1}. \quad (\text{S14})$$

The modified Kramers-Moyal coefficients  $A_n(\nu)$  defined in Eq. (8) of the main text becomes

$$\begin{aligned} A_n(\nu) = & S\rho \left(\frac{M}{\gamma}\right) \int d\phi F(\phi) \frac{1}{2} \sqrt{\frac{2k_B T}{\pi m}} (-\eta\beta)^{-n} e^{-\eta^2 \nu^2} \left[ \Gamma\left(1 + \frac{n}{2}\right) \Phi\left(1 + \frac{n}{2}, \frac{1}{2}, \eta^2 \nu^2\right) \right. \\ & \left. + 2\eta\nu \Gamma\left(\frac{3+n}{2}\right) \Phi\left(\frac{3+n}{2}, \frac{3}{2}, \eta^2 \nu^2\right) \right] - G(\nu) \nu \delta_{n,1} \end{aligned} \quad (\text{S15})$$

where  $\eta = v_0 \alpha = \epsilon \sin \phi / \sqrt{2}$ .

In the small mass-ratio limit ( $\epsilon \ll 1$ ),  $A_n(\nu)$  can be expanded in terms of  $\epsilon$  as

$$\begin{aligned} A_n(\nu) = & S\rho \left(\frac{M}{\gamma}\right) (-1)^n 2^{\frac{3}{2}n} \sqrt{\frac{k_B T}{2\pi m}} \left[ \Gamma\left(1 + \frac{n}{2}\right) \langle \sin^n \phi \rangle_F \epsilon^n + \sqrt{2} \Gamma\left(\frac{3+n}{2}\right) \langle \sin^{n+1} \phi \rangle_F \nu \epsilon^{n+1} \right. \\ & \left. + \Gamma\left(1 + \frac{n}{2}\right) \langle \sin^{n+2} \phi \rangle_F \left(-n + \frac{1}{2}(1+n)\nu^2\right) \epsilon^{n+2} + \mathcal{O}(\epsilon^{n+3}) \right] - G(\nu) \nu \delta_{n,1}, \end{aligned} \quad (\text{S16})$$

where the geometric factors are given as

$$\langle \sin^n \phi \rangle_F \equiv \int_0^{2\pi} d\phi \sin^n \phi F_\phi = \frac{L}{S} [1 - (-\sin \theta)^{n-1}] \quad (n = 1, 2, \dots) \quad (\text{S17})$$

with the form factor  $F_\phi$  in Eq. (S5). It would be easily generalized for an arbitrary convex shape by calculating the corresponding form factor. The friction coefficient  $\gamma$  is determined from the average equation of motion for the t-particle as  $M\langle\dot{v}\rangle = -\gamma\langle v\rangle$ , which is identical to the condition on the first Kramer-Moyal coefficient as  $a_1(v) = -(\gamma/M)v$  or equivalently  $A_1(\nu) = -\nu - G(\nu)\nu$  to the lowest order in  $\epsilon$ . From Eq. (S16), it is easy to identify

$$\gamma = 4S\rho\sqrt{\frac{mk_B T}{2\pi}}\langle\sin^2\phi\rangle_F = 4L\rho\sqrt{\frac{mk_B T}{2\pi}}(1 + \sin\theta). \quad (\text{S18})$$

With this  $\gamma$ , the first few coefficients  $A_n(\nu)$  can be easily obtained up to  $\mathcal{O}(\epsilon)$  and given in Eq. (9) of the main text with the asymmetric factor  $\bar{a}$  as

$$\bar{a} = \frac{\sqrt{2\pi}\langle\sin^3\phi\rangle_F}{4\langle\sin^2\phi\rangle_F} = \frac{\sqrt{2\pi}}{4}(1 - \sin\theta). \quad (\text{S19})$$

Note that both  $\gamma$  and  $\bar{a}$  depend on the form factor, thus the shape of the active object.

### III. ANALYTIC RESULTS FOR ACTIVE MODELS

Here we present the explicit calculations for the steady-state velocity and its fluctuation up to  $\mathcal{O}(\epsilon)$  for the simple, the RH, the depot, and the SG models. We use the formulae given in Eqs. (12), (13), and (14) of the main text with  $G(\nu) = \Gamma(v_0\nu)/\gamma$  for each model as

$$G^{\text{sim}}(\nu) = \hat{\Gamma}, \quad G^{\text{RH}}(\nu) = \hat{\Gamma} + \Omega\nu^2, \quad G^{\text{dpt}}(\nu) = \hat{\Gamma}/(1 + Z\nu^2), \quad G^{\text{SG}}(\nu) = \hat{\Gamma}/|\nu|, \quad (\text{S20})$$

with dimensionless parameters  $\hat{\Gamma} = \hat{\gamma}/\gamma$ ,  $\Omega = \omega v_0^2/\gamma$ , and  $Z = \zeta v_0^2$ .

First, for the simple model, we obtain

$$P_s^{\text{sim},(0)}(\nu) = \frac{1}{\mathcal{N}^{\text{sim}}}e^{-\frac{1+\hat{\Gamma}}{2}\nu^2} \quad \text{and} \quad g^{\text{sim}}(\nu) = 2\hat{\Gamma}\nu - \frac{\hat{\Gamma}}{3}\left(1 + 2\hat{\Gamma}\right)\nu^3, \quad (\text{S21})$$

with the normalization factor  $\mathcal{N}^{\text{sim}} = \sqrt{2\pi/(1 + \hat{\Gamma})}$ . Then the steady-state velocity becomes

$$\langle\nu\rangle_s^{\text{sim}} \approx \bar{a}\epsilon \left[ 2\hat{\Gamma}\langle\nu^2\rangle_0^{\text{sim}} - \frac{\hat{\Gamma}}{3}\left(1 + 2\hat{\Gamma}\right)\langle\nu^4\rangle_0^{\text{sim}} \right] = \bar{a}\epsilon \frac{\hat{\Gamma}}{1 + \hat{\Gamma}}\langle\nu^2\rangle_0^{\text{sim}} = \bar{a}\epsilon \frac{\hat{\Gamma}}{(1 + \hat{\Gamma})^2}, \quad (\text{S22})$$

where we used the Gaussian integral property of  $\langle\nu^4\rangle_0^{\text{sim}} = 3(\langle\nu^2\rangle_0^{\text{sim}})^2$  and  $\langle\nu^2\rangle_0^{\text{sim}} = \frac{1}{1+\hat{\Gamma}}$ . Its second moment becomes

$$\langle\nu^2\rangle_s^{\text{sim}} \approx \langle\nu^2\rangle_0^{\text{sim}} = \frac{1}{1 + \hat{\Gamma}}. \quad (\text{S23})$$



For the RH model, we obtain

$$P_s^{\text{RH},(0)}(\nu) = \frac{1}{\mathcal{N}^{\text{RH}}} e^{-\frac{1+\hat{\Gamma}}{2}\nu^2 - \frac{\Omega}{4}\nu^4}$$

and  $g^{\text{RH}}(\nu) = 2\hat{\Gamma}\nu + \left(2\Omega - \frac{1}{3}\hat{\Gamma} - \frac{2}{3}\hat{\Gamma}^2\right)\nu^3 - \frac{1}{5}\left(1 + 4\hat{\Gamma}\right)\Omega\nu^5 - \frac{2}{7}\Omega^2\nu^7,$  (S24)

with the normalization factor  $\mathcal{N}^{\text{RH}} = \int_{-\infty}^{\infty} d\nu e^{-\frac{1+\hat{\Gamma}}{2}\nu^2 - \frac{\Omega}{4}\nu^4}$ . Then, the steady-state velocity becomes

$$\langle \nu \rangle_s^{\text{RH}} \approx \bar{a}\epsilon \left[ 2\hat{\Gamma}\langle \nu^2 \rangle_0^{\text{RH}} + \left(2\Omega - \frac{1}{3}\hat{\Gamma} - \frac{2}{3}\hat{\Gamma}^2\right)\langle \nu^4 \rangle_0^{\text{RH}} - \frac{1}{5}\left(1 + 4\hat{\Gamma}\right)\Omega\langle \nu^6 \rangle_0^{\text{RH}} - \frac{2}{7}\Omega^2\langle \nu^8 \rangle_0^{\text{RH}} \right].$$
 (S25)

The normalization  $\mathcal{N}^{\text{RH}}$  and the moments  $\langle \nu^n \rangle_0^{\text{RH}}$  can be calculated numerically. It is useful to rewrite all higher moments in terms of the second moment. Using the simple recurrence relations as  $(n+1)\langle \nu^n \rangle_0^{\text{RH}} = (1+\hat{\Gamma})\langle \nu^{n+2} \rangle_0^{\text{RH}} + \Omega\langle \nu^{n+4} \rangle_0^{\text{RH}}$  for  $n = 0, 2, 4, \dots$  (easily derived by the integration by parts), we find for finite  $\Omega$

$$\langle \nu \rangle_s^{\text{RH}} \approx \frac{\bar{a}\epsilon}{105\Omega} \left[ 60\Omega - 9 + 10\hat{\Gamma} - 16\hat{\Gamma}^2 - \left( (33 + 12\hat{\Gamma})\Omega - (9 - 10\hat{\Gamma} + 16\hat{\Gamma}^2)(1 + \hat{\Gamma}) \right) \langle \nu^2 \rangle_0^{\text{RH}} \right].$$
 (S26)

Thus, the average velocity can be calculated from the numerical estimation of the zeroth-order second moment  $\langle \nu^2 \rangle_0^{\text{RH}}$ , and its second moment is simply given by  $\langle \nu^2 \rangle_s^{\text{RH}} \approx \langle \nu^2 \rangle_0^{\text{RH}}$  up to  $\mathcal{O}(\epsilon)$ . One can show their asymptotic behaviors for large  $\hat{\Gamma}$  as

$$\langle \nu \rangle_s^{\text{RH}} \simeq \frac{\bar{a}\epsilon}{\hat{\Gamma}}, \quad \langle \nu^2 \rangle_s^{\text{RH}} \simeq \frac{1}{\hat{\Gamma}} \quad \text{for } \hat{\Gamma} \rightarrow +\infty$$

and  $\langle \nu \rangle_s^{\text{RH}} \simeq -\frac{16\bar{a}\epsilon}{105} \left( \frac{\hat{\Gamma}^4}{\Omega^2} \right), \quad \langle \nu^2 \rangle_s^{\text{RH}} \simeq \frac{|\hat{\Gamma}|}{\Omega} \quad \text{for } \hat{\Gamma} \rightarrow -\infty.$  (S27)

Note that the asymptotic behavior for positive  $\hat{\Gamma}$  is identical to that of the simple model.

For the depot model, we obtain

$$P_s^{\text{dpt},(0)}(\nu) = \frac{1}{\mathcal{N}^{\text{dpt}}} e^{-\frac{1}{2}\nu^2} (1 + Z\nu^2)^{-\frac{\hat{\Gamma}}{2Z}}$$

and  $g^{\text{dpt}}(\nu) = -\frac{\hat{\Gamma}}{Z}\nu + \frac{\hat{\Gamma}(2Z + \hat{\Gamma})}{Z} \frac{\nu}{1 + Z\nu^2} + \frac{\hat{\Gamma}(1 - \hat{\Gamma})}{Z\sqrt{Z}} \tan^{-1}(\sqrt{Z}\nu),$  (S28)

with the normalization factor  $\mathcal{N}^{\text{dpt}}$ . Then, the steady-state velocity of the depot model becomes

$$\langle \nu \rangle_s^{\text{dpt}} \approx \bar{a}\epsilon \left[ -\frac{\hat{\Gamma}}{Z}\langle \nu^2 \rangle_0^{\text{dpt}} + \frac{\hat{\Gamma}(2Z + \hat{\Gamma})}{Z} \left\langle \frac{\nu^2}{1 + Z\nu^2} \right\rangle_0^{\text{dpt}} + \frac{\hat{\Gamma}(1 - \hat{\Gamma})}{Z\sqrt{Z}} \left\langle \nu \tan^{-1}(\sqrt{Z}\nu) \right\rangle_0^{\text{dpt}} \right].$$
 (S29)

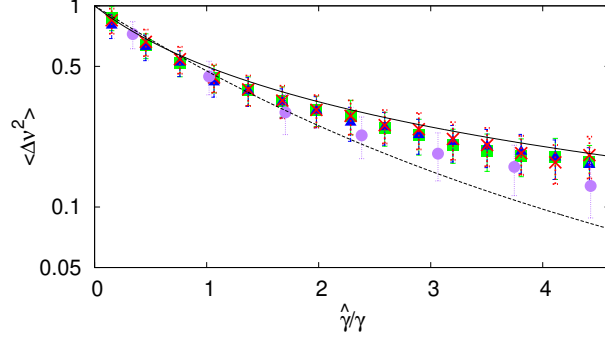


FIG. S8. Fluctuations as a function of  $\hat{\gamma}/\gamma$ . Solid and dashed curves correspond to the simple and the SG models in Eq. (S22) and Eq. (S32), respectively. Green  $\blacksquare$ , blue  $\blacktriangle$ , red  $\times$ , and purple  $\bullet$  points denote numerical data for the simple, the RH, the depot, and the SG models, respectively.

with  $\langle \nu^2 \rangle_s^{\text{dpt}} \approx \langle \nu^2 \rangle_0^{\text{dpt}}$ . It is not possible to rewrite this expression in a simpler form, so we perform numerical integrations directly. The asymptotic behaviors are similar to those for the RH model in Eq. (S27).

For the SG model, we obtain

$$P_s^{\text{SG},(0)}(\nu) = \frac{1}{\mathcal{N}^{\text{SG}}} e^{-\frac{1}{2}\nu^2 - \hat{\Gamma}|\nu|} \quad \text{and} \quad g^{\text{SG}}(\nu) = 2\hat{\Gamma} \frac{\nu}{|\nu|} - 2\hat{\Gamma}^2 \nu - \frac{1}{2}\hat{\Gamma} \nu |\nu|, \quad (\text{S30})$$

with the normalization factor  $\mathcal{N}^{\text{SG}} = \sqrt{2\pi} e^{\frac{1}{2}\hat{\Gamma}^2} \text{erfc}\left(\frac{\hat{\Gamma}}{\sqrt{2}}\right)$  where the complimentary error function is defined as  $\text{erfc}(x) = \frac{2}{\sqrt{\pi}} \int_x^\infty ds e^{-s^2}$ . Then, the steady-state velocity becomes

$$\langle \nu \rangle_s^{\text{SG}} = \bar{a}\epsilon \left( 2\hat{\Gamma} \langle |\nu| \rangle_0^{\text{SG}} - 2\hat{\Gamma}^2 \langle |\nu|^2 \rangle_0^{\text{SG}} - \frac{1}{2}\hat{\Gamma} \langle |\nu|^3 \rangle_0^{\text{SG}} \right). \quad (\text{S31})$$

Again, we find useful recurrence relations as  $\langle |\nu|^n \rangle_0^{\text{SG}} = (n-1) \langle |\nu|^{n-2} \rangle_0^{\text{SG}} - \hat{\Gamma} \langle |\nu|^{n-1} \rangle_0^{\text{SG}} + (2/\mathcal{N}^{\text{SG}}) \delta_{n,1}$  for  $n = 1, 2, \dots$  (by simple integrations by parts). Then, we obtain a simplified form for  $\langle \nu \rangle_s^{\text{SG}}$  as

$$\langle \nu \rangle_s^{\text{SG}} = \frac{\bar{a}\epsilon \hat{\Gamma}}{2} \left( -3\hat{\Gamma} + (2 + 3\hat{\Gamma}^2) \langle |\nu| \rangle_0^{\text{SG}} \right) = \frac{\bar{a}\epsilon \hat{\Gamma}}{2} \left( -5\hat{\Gamma} - 3\hat{\Gamma}^3 + \frac{4 + 6\hat{\Gamma}^2}{\mathcal{N}^{\text{SG}}} \right). \quad (\text{S32})$$

with the second moment

$$\langle \nu^2 \rangle_s^{\text{SG}} \approx \langle |\nu|^2 \rangle_0^{\text{SG}} = 1 + \hat{\Gamma}^2 - \frac{2\hat{\Gamma}}{\mathcal{N}^{\text{SG}}}. \quad (\text{S33})$$

Their asymptotic behaviors are given as

$$\begin{aligned} \langle \nu \rangle_s^{\text{SG}} &\simeq \bar{a}\epsilon \left( -2 + \frac{13}{\hat{\Gamma}^2} \right), \quad \langle \nu^2 \rangle_s^{\text{SG}} \simeq \frac{2}{\hat{\Gamma}^2} \quad \text{for } \hat{\Gamma} \rightarrow +\infty \\ \text{and } \langle \nu \rangle_s^{\text{SG}} &\simeq -\frac{3\bar{a}\epsilon}{2} \hat{\Gamma}^4, \quad \langle \nu^2 \rangle_s^{\text{SG}} \simeq \hat{\Gamma}^2 \quad \text{for } \hat{\Gamma} \rightarrow -\infty. \end{aligned} \quad (\text{S34})$$

#### IV. ESTIMATION OF THE PARAMETER VALUES FOR BIOLOGICAL OBJECTS

We estimate the parameter values in real experimental situations. Consider a bacterium like *E. coli* in water-rich medium at room temperature. The small expansion parameter  $\epsilon = \sqrt{m/M} \simeq 5 \times 10^{-6}$  with  $m = 3.0 \times 10^{-26}$  kg (water molecule mass) and  $M = 10^{-15}$  kg (*E. coli* mass) [9]. The velocity unit  $v_0 = \sqrt{k_B T/M} \simeq 2.0 \times 10^{-3}$  m/s with  $T = 300$  K. We take the asymmetric factor  $\bar{a} = \sqrt{2\pi}(1 - \sin\theta)/4 \simeq 0.2$  for  $\theta = \pi/4$ . As can be seen in Eqs. (5) and (14) of the main text, the magnitude of the rectified velocity is given as  $\langle v \rangle_s = v_0 \bar{a} \epsilon \langle \nu g(\nu) \rangle_0$  with  $v_0 \bar{a} \epsilon \simeq 2$  nm/s.

As the self-propelling speed of a typical bacterium is  $\sim 10$   $\mu\text{m/s}$ , the rectification effect due to the shape asymmetry seems negligible in the passive mode where  $\langle \nu g(\nu) \rangle_0 \sim \mathcal{O}(1)$ . However, in the active mode, this factor can grow indefinitely as  $\hat{\Gamma} = \hat{\gamma}/\gamma$  becomes larger in the negative side, see Fig. 2 of the main text and Eqs. (S27) and (S34). For example, we can read from Fig. 2 (a) of the main text that the rectification speed is  $\sim 2\mu\text{m/s}$  at  $\hat{\Gamma} \simeq -2$ , which is already comparable to the self-propelling speed.

For smaller (lighter) objects like a virus or a molecular motor,  $v_0 \bar{a} \epsilon \simeq 2\mu\text{m/s}$  (2 mm/s) for  $M = 10^{-18}$  ( $10^{-21}$ ) kg for a HIV-1 virus (ATP synthase). Their speed is big enough for performing relevant biological operations, even in the passive mode including the mbd (moving by dissipation) regime.

#### V. APEX-ANGLE-DEPENDENT BEHAVIOR

In the main text, we fix the apex angle  $\theta = \pi/4$ . Here we discuss the role of the apex angle for  $0 < \theta < \pi/2$  on the magnitude and direction of the rectified velocity.

As we change  $\theta$  from 0 to  $\pi/2$ , the friction coefficient  $\gamma$  increases as in Eq. (S18), while the asymmetric factor decreases as in Eq. (S19). This leads to an interesting nontrivial behavior of the steady-state velocity  $\langle \nu \rangle_s$ . Figure S9 shows  $\hat{\gamma}$  and  $\theta$  dependent behavior of  $\langle \nu \rangle_s$ , where  $\hat{\gamma}$  is rescaled by the friction coefficient for the symmetric particle  $\gamma|_{\theta=\pi/2} = 8L\rho\sqrt{(mk_B T)/(2\pi)}$ . For the depot model, Figs. S9 (c) and (d) show that the magnitude  $|\langle \nu \rangle_s|$  monotonically increases as  $\theta$  decreases (more asymmetric) for finite  $\hat{\gamma}$ . However, for the RH model, the velocity magnitude behaves non-monotonically and the direction change

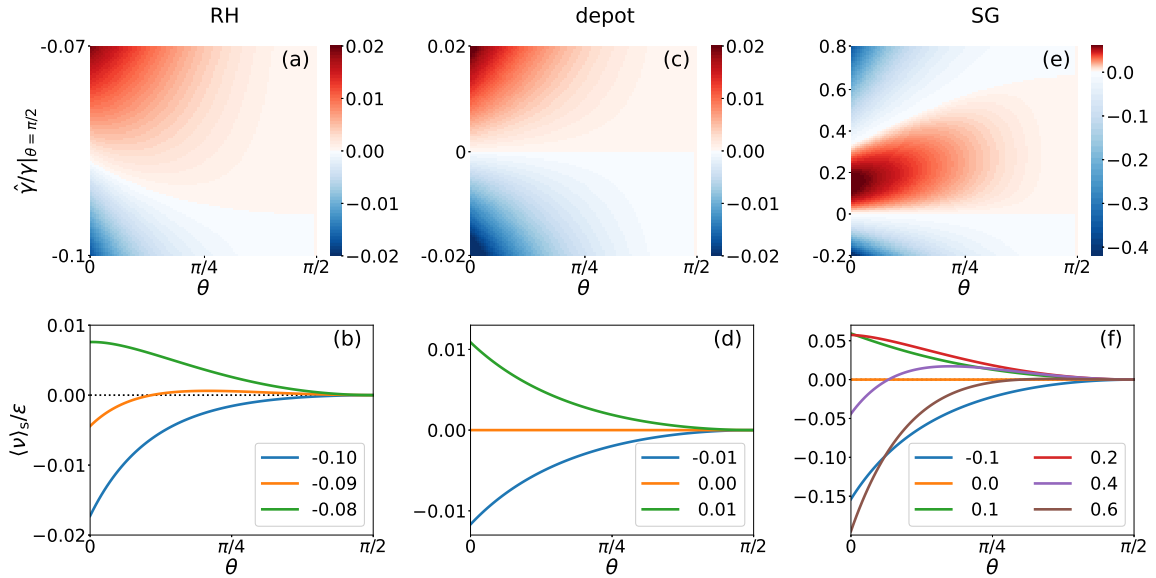


FIG. S9.  $\hat{\gamma}$  and  $\theta$  dependence of the rectified velocity  $\langle \nu \rangle_s$ . Upper panels show the rescaled steady-state velocity  $\langle \nu \rangle_s / \epsilon$  as a function of the dimensionless parameter  $\hat{\gamma}/\gamma|_{\theta=\pi/2}$  and the apex angle  $\theta$  for (a) the RH, (c) the depot, and (e) the SG models. Lower panels show the  $\theta$  dependence of the velocity  $\langle \nu \rangle_s / \epsilon$  for various  $\hat{\gamma}$  values of the dimensionless parameter  $\hat{\gamma}/\gamma|_{\theta=\pi/2}$ : (b)  $\hat{\gamma}/\gamma|_{\theta=\pi/2} = -0.1$  (blue),  $-0.09$  (orange), and  $-0.08$  (green) for the RH model, (d)  $-0.01$  (blue),  $0$  (orange), and  $0.01$  (green) for the depot model, and (f)  $-0.1$  (blue),  $0$  (orange),  $0.1$  (green),  $0.2$  (red),  $0.4$  (violet), and  $0.6$  (brown) for the SG model. The black dotted line indicates  $\langle \nu \rangle_s / \epsilon = 0$ .

happens within a narrow range near  $\hat{\gamma}/\gamma|_{\theta=\pi/2} \approx -0.09$  as shown in Figs. S9 (a) and (b). The SG model also exhibits a non-monotonic behavior of the velocity as shown in Figs. S9 (e) and (f).

Overall, we find that an active object moves faster in general as its shape becomes more asymmetric (sharper) with fixed  $\hat{\gamma}$  for a wide range of  $\hat{\gamma}$ . This indicates that an active object can make use of the shape change to accelerate or decelerate its velocity. Furthermore, as learned from the RH and SG models, it can easily change the direction of motion by deforming their shape with a fine-tuned value of  $\hat{\gamma}$ .

---

[1] C. Van den Broeck, R. Kawai, and P. Meurs, Microscopic Analysis of a Thermal Brownian Motor, Phys. Rev. Lett. **93**, 090601 (2004).

- [2] J. Lee and H. Park, Additivity of multiple heat reservoirs in the Langevin equation, *Phys. Rev. E* **97**, 062135 (2018).
- [3] G. S. Grest and K. Kremer, Molecular dynamics simulation for polymers in the presence of a heat bath, *Phys. Rev. A* **33**, 3628(R) (1986).
- [4] H. Risken, *The Fokker-Planck Equation* (Springer, Berlin, 1989).
- [5] N. G. van Kampen, *Stochastic Processes in Physics and Chemistry* (Elsevier, 2007).
- [6] P. Romanczuk, M. Bär, W. Ebeling, B. Lindner, and L. Schimansky-Geier, Active Brownian Particles. From Individual to Collective Stochastic Dynamics, *Eur. Phys. J. Special Topics* **202**, 1162 (2012).
- [7] Y. Fily and M. C. Marchetti, Athermal Phase Separation of Self-Propelled Particles with No Alignment, *Phys. Rev. Lett.* **108**, 235702 (2012).
- [8] P. Meurs, C. Van den Broeck, and A. Garcia, Rectification of thermal fluctuations in ideal gases, *Phys. Rev. E* **70**, 051109 (2004).
- [9] R. Milo and R. Phillips, *Cell Biology by the Numbers* (CRC Press, 2015).